Reference: *Biol. Bull.* **215:** 295–308. (December 2008)

Flow Forces on Seaweeds: Field Evidence for Roles of Wave Impingement and Organism Inertia

BRIAN GAYLORD[1,*], MARK W. DENNY[2], AND M. A. R. KOEHL[3]

[1]*Bodega Marine Laboratory and Department of Evolution and Ecology, University of California at Davis, Bodega Bay, California 94923;* [2]*Department of Biological Sciences, Stanford University, Hopkins Marine Station, Pacific Grove, California 93950; and* [3]*Department of Integrative Biology, University of California at Berkeley, Berkeley, California 94720-3140*

Abstract. Hydrodynamic forces dislodge and kill large numbers of organisms in intertidal and subtidal habitats along rocky shores. Although this feature of wave-driven water motion is well recognized, the mechanics of force imposition on compliant organisms is incompletely understood. Here we undertake a field examination of two processes that are thought to impose many of the more dangerous forces that act on flexible benthic seaweeds: impingement of breaking waves directly on emergent organisms, and inertial effects tied to the rapid deceleration of mass that occurs when a passively moving but attached organism abruptly reaches the extent of its range of motion. We focus on two common and important seaweed species: one intertidal kelp (*Egregia menziesii*) and one subtidal kelp (*Macrocystis pyrifera*). Results support the concept that wave impingement and inertial effects produce intermittent force transients whose magnitudes commonly exceed values readily attributable to drag. Peak force transients are elevated by as much as a factor of 3 relative to drag in both small and large individuals, consistent with smaller seaweeds being more susceptible to brief impingement forces, and larger seaweeds being more vulnerable to inertial forces. Because both wave impingement and inertial effects vary with the size of an organism, they may have the potential to influence the demographics of physical disturbance in an array of flexible species.

Received 25 January 2008; accepted 27 July 2008.

* To whom correspondence should be addressed. E-mail: bpgaylord@ucdavis.edu

Introduction

Physical disturbance is a critical structuring agent in many intertidal and subtidal communities (Sousa, 1985, 2001). This point has spurred a growing list of studies examining the mechanics, scaling implications, and ecology of force imposition on coastal benthic organisms (*e.g.,* Koehl, 1977; Denny *et al.,* 1985; Carrington, 1990; Dudgeon and Johnson, 1992; Gaylord *et al.,* 1994; Stevens *et al.,* 2002; Stewart, 2006). Despite such attention, important questions remain, particularly about flexible organisms where processes of force application are complicated by passive reorientation of the plant or animal in flow. Such organisms often experience smaller forces than would be expected from their maximal projected areas, since they can reconfigure into streamlined shapes (Koehl, 1982; Vogel, 1984). Dynamic mechanisms of force modification may also operate. Passively moving seaweeds exposed to waves flap back and forth as they "go with the flow," experiencing substantial water motion relative to their own tissues only after they reach the ends of their tethers (Koehl, 1984, 1986; Johnson and Koehl, 1994). Movement can also increase a seaweed's vulnerability to "jerk"-like inertial forces associated with the rapid deceleration of the organism's mass when it reaches the extent of its range of motion (Gaylord and Denny, 1997; Denny *et al.,* 1997, 1998).

Characteristics of the physical environment further modulate magnitudes of imposed force. Peak velocities are often an order of magnitude higher under breaking waves in intertidal regions than in deeper, subtidal areas (Denny, 1985; Gaylord, 1999). It is probably no coincidence that forests of the giant kelp (*Macrocystis pyrifera*) are therefore confined to depths beyond the surf zone (Seymour *et al.,* 1989; Graham, 1997). Despite obvious flow differences

between intertidal and subtidal areas, however, only recently have biologists begun to appreciate that mechanisms of force imposition may differ distinctly between these two environments. Drag is the usual focus in biomechanical studies involving fluid forces; its relatively simple relationship to the velocity past an organism is widely known (Vogel, 1994). In intertidal areas, however, other flow forces—in particular brief forces associated with the initial impingement of waves on emergent organisms—can impose additional forces (Gaylord, 2000). Such impingement forces do not arise under unbroken waves in subtidal habitats (Denny and Gaylord, 2002).

Despite experimental clues and theoretical justification for roles of non-drag effects like inertial forces and wave impingement (Denny *et al.,* 1998; Gaylord, 2000; Wolcott, 2007), there are relatively few explicit data concerning these mechanisms (Gaylord, 2000; Boller and Carrington, 2006). Our goal in the present study is to address this gap, using deviations of force from values associated with classic drag as key indicators of underlying traits in the hydrodynamic interactions. To this end, we recorded high-resolution field measurements of flow forces imposed on two common kelps that are major space occupiers on many temperate rocky shores. *Egregia menziesii* (the feather-boa kelp) is a robust intertidal seaweed that has a simple growth form characterized by a straplike morphology. Tissue mass is added only as fronds of nearly constant cross-sectional area get longer, which minimizes complications in this species' allometric relationships. *Macrocystis pyrifera* is an important subtidal, habitat-forming species (Dayton, 1972) that proliferates its canopy upon reaching the water's surface. The large canopy makes this species a preferred choice for examining details of inertial effects. We therefore used *E. menziesii* and *M. pyrifera* as case examples for examining the importance of wave impingement and inertial processes across a range of seaweed size.

Materials and Methods

Species and field sites

Individuals of *Egregia menziesii* (Turner) were collected during 5 May–5 July 2004 from the mid-intertidal zone at Cabrillo Point, a rocky headland within Hopkins Marine Station (HMS), Pacific Grove, California (36°37′18″N, 121°54′15″W). This site sits inside Monterey Bay and so is protected from the full brunt of winter storms, but experiences large waves on occasion. The *E. menziesii* specimens spanned the full range of sizes occurring at HMS, and included individuals with few to many fronds (called rachises, although we avoid use of this specialized term), some with buoyant bladders (pneumatocysts) and others without. The gross morphology of the sampled kelps corresponded to that of the "northern form" of Abbott and Hollenberg (1976) and Blanchette *et al.* (2002). Each individual was collected by prying its holdfast free from the rock, taking care to avoid damaging any portion of the organism. Specimens were re-deployed in the field for testing within 1 h of collection.

Individuals of *Macrocystis pyrifera* (L.) C. Agardh were collected during 17–20 October 2005 from populations near Santa Barbara, California (34°23′38″N, 119°43′45″W). This region is in the lee of Point Conception, a major geographic feature of the California coast, which protects the study site from large waves generated by most winter storms. As at the HMS site, however, intense storms impinge sporadically on Santa Barbara kelp forests, making large waves occasional but important features of their environment (Ebeling *et al.,* 1985). Because *M. pyrifera* holdfasts cannot be easily pried from the substratum without tearing their haptera, individuals of this species were collected by cutting through the bases of their holdfasts at the level of the substratum, using a fine-tooth saw. This procedure left less than 5% of the holdfast behind. Each *M. pyrifera* specimen was tested in the field within 2 h of collection.

Intertidal force measurements on Egregia menziesii

Hydrodynamic forces acting on *E. menziesii* individuals subjected to breaking waves were recorded using a coupled flow-and-force apparatus similar to that of Gaylord (2000). A three-axis cantilever-style force sensor was mounted flush with the surrounding substratum inside a concrete emplacement built into the rock in the mid-intertidal zone at HMS. The holdfast of each *E. menziesii* individual was lashed tightly to the force sensor's mounting plate, positioning the kelp in its natural orientation to the substratum. As waves impinged on the seaweed, the sensor produced voltage signals proportional to force that were carried by electronic cable to a laptop computer located in a protected structure 50 m up the shore. The signals were low-pass filtered at 20 Hz, passed through an instrumentation amplifier and analog-to-digital converter (Fylde Electronics), then recorded at 50 Hz (Labview software ver. 7.0, National Instruments). This sampling protocol prevented digital aliasing and eliminated unwanted signal components associated with minor vibration of the cantilever elements at their natural frequencies (≈50 Hz, quantified by tracking free vibrations resulting from application of a force impulse). Twelve 10-min sessions were recorded for each experimental individual over the course of a full (≈24-h) tidal cycle.

A drag-sphere flow probe (Gaylord, 1999) that recorded velocities along the three coordinate axes was positioned 40 cm away from the force sensor along a line parallel to the incident wave crests. This placement ensured that waves arrived at the force sensor and flow probe as simultaneously as feasible, although slight temporal differences inevitably arose due to the chaotic nature of flows in the surf zone. A

wire cage (2.5-cm mesh; Miller and Gaylord, 2007) protected the flow probe from the whiplash of nearby seaweeds. Voltage signals from the flow probe were carried *via* electronic cable to the laptop, and were filtered and sampled in the same way as for the force sensor.

The force sensor was calibrated in the laboratory by hanging weights of known mass from the mounting plate along each of the three coordinate axes. The slopes of the resulting linear regressions provided the conversion factors between voltage and force (all r^2 values > 0.99). Cross-talk among axes was less than 1%, verified by applying forces successively to each axis and observing the responses of the other axes. The flow probe was calibrated in the field, within its protective cage, by positioning it immediately adjacent to an acoustic Doppler velocimeter (ADV; Nortek USA) at a depth of 2 m under nonbreaking waves. The conversion factor was computed as the coefficient that yielded a slope of 1.0 when the voltage record from the flow probe was regressed against the square of velocity from the ADV ($r^2 = 0.86$).

Subtidal force measurements on Macrocystis pyrifera

Techniques analogous to those used intertidally were employed to record forces imposed on subtidal *M. pyrifera* individuals in waters of 6–7 m depth. A larger version of the intertidal force sensor was constructed, enabling attachment of giant kelp with holdfast diameters up to 0.5 m across. The subtidal force sensor was held within a housing embedded in the sand, ensuring that its mounting plate was flush with the seabed. An electronic cable carried voltage signals to a laptop computer on a boat moored 50 m away, where the signals were filtered at 20 Hz, amplified, passed through an analog-to-digital converter, and recorded at 100 Hz for 20 min. This sampling protocol prevented digital aliasing, and although the natural frequencies of vibration ($\approx$25 Hz) for the subtidal force sensor were near the filter cutoff, spectral analysis of the recordings indicated negligible energy at such frequencies. An ADV, sampling at 4 Hz, was mounted 2.2 m away from the kelp along a line parallel to the wave crests, providing a record of the three components of velocity at a height 1.5 m above the seafloor during the same time period. The subtidal force sensor was calibrated using weights of known mass as for the intertidal force sensor, and cross-talk among axes was also verified to be less than 2%. The ADV maintains a factory-fixed calibration.

Morphological characteristics

Morphological traits of each experimental kelp were quantified by weighing its fronds and holdfast, recording the number and lengths of its fronds, and using one of two simple techniques to determine its maximal projected area (*i.e.,* the maximal area that could face flow if the kelp was configured in its least streamlined posture). Each individual of *E. menziesii* was splayed flat on the ground with every frond separated from its neighbors, then photographed from above. Effects of parallax were minimized by shooting from atop a 3-m ladder. The photographs were analyzed digitally, tracing the outline of each kelp using image processing software (Image J ver. 1.37, National Institutes of Health). The much greater projected areas of *M. pyrifera* made photography impractical; instead, the blades were detached from the stipes, and blades and stipes were arrayed like jigsaw pieces flush against one another on the ground, filling a rectangular region. The area of this region (length times width) was used as an estimate of the maximal projected area of the kelp. Total volume, V, was determined by dividing its mass by a typical tissue density for kelps (1050 kg/m^3; Gaylord and Denny, 1997). The measured volumes and projected areas of the kelps were then combined to compute a so-called flatness index, $A^{3/2}/V$, a nondimensional representation of the degree to which a seaweed grows as a flat sheet *versus* a more three-dimensional structure (Gaylord, 2000).

Attributes of the focal forces

Seaweeds of varying morphology interact with flow in different ways and can be subjected to distinct forces that operate according to their own rules. Drag is typically represented *via* the classic equation of introductory fluid dynamics

$$F_d = 0.5\rho A C_d u^2 \quad (1)$$

where F_d is drag, ρ is fluid density, A is a reference area (which for flexible organisms is often taken as the maximal possible area that could face flow), C_d is a dimensionless shape factor termed the drag coefficient, and u is velocity relative to the organism (Vogel, 1994). This expression is strictly applicable to any organism immersed in a moving fluid. However, Eq. 1 is often less than ideal for flexible seaweeds whose instantaneous geometries and projected areas change as they reorient and reconfigure in flow. Such fluid-induced responses result in drag coefficients that typically vary with velocity raised to a negative power (Vogel, 1984, 1989). For seaweeds, a more efficient representation of drag can therefore be achieved by replacing the term $C_d u^2$ (where C_d is an exceptionally strong function of u) with the expression $S_d u^\gamma$, yielding

$$F_d = 0.5\rho A S_d u^y \quad (2)$$

The advantage of Eq. 2 is that both S_d and γ serve as invariant constants across a wide range of velocity (Denny, 1995).

Wave impingement and inertial effects arise in ways that differ from drag. Inertial forces are imposed when, in accordance with Newton's Second Law, the mass, m, of a

seaweed is decelerated at rate, a, by its own attachment structure as it reaches the maximum extent of its range of motion

$$F_{inertia} = ma \tag{3}$$

Impingement forces, on the other hand, result from the need for fluid streamlines to evolve rapidly into a novel pattern of flow when a wave impacts an obstructing organism. The origin of the additional force that ensues is apparent from Euler's equation, an alternative form of Newton's Second Law appropriate for fluids (Gaylord, 2000)

$$-\frac{dp}{dx} = \rho\left(\frac{\partial u}{\partial t} + u\frac{\partial u}{\partial x}\right) \tag{4}$$

where dp/dx is the pressure gradient along the axis of flow that ultimately leads to the upstream-downstream pressure difference that applies a force to an organism. The term in brackets is the total derivative, du/dt, expanded in terms of its partial derivatives to emphasize the dependence of the velocity field on both time and space. Under conditions of steady flow, the first term in brackets is zero and drag alone operates. When a wave first impinges on an organism, however, the first term in brackets becomes large, adding to the second term and producing a more extreme pressure gradient. A greater force (*i.e.,* the impingement force) then results.

Overview of the data analyses

Meeting the core purpose of the field measurements (*i.e.,* evaluating the potential importance of wave impingement and organism inertia relative to drag, as a function of seaweed size) requires distinguishing drag from other agents of force application. This task is complex and involves a somewhat nuanced methodology that we approached in three steps. First, we quantified best-fit values of S_d and γ describing the relationship between flow speed and drag. We exploited in this context the fact that transients potentially produced by non-drag factors are sufficiently brief that they have minimal effect on the lowest-order moments (means) of the force distributions associated with given flow speeds. Second, we applied the calculated drag parameters (S_d and γ) back to the velocity data, in much the same way as a mathematical "transfer function," to convert from water velocity to predicted drag. This step yielded a quantitative estimate of the drag distributions one would expect based purely on measured velocities. Although effects of seaweed reconfiguration and reposturing are only incompletely modeled by this procedure, thereby contributing to discrepancies between the predicted drag and actual force distributions, they do not readily cause predicted drag distributions to differ from measured force distributions in a manner that depends on seaweed size. This latter point was exploited in the third step of the analysis, where predicted drag distributions were compared to the measured force distributions across a range of seaweed size. We focused on the tails of the distributions, taking ratios of specific percentile values of measured force to the same percentile values of predicted drag. The rationale was that if only drag was important, then the ratios of measured force to predicted drag should remain effectively constant across a range of seaweed size, as was alluded to above. If, on the other hand, specific patterns in the ratios arose as a function of seaweed size, this outcome would be consistent with non-drag mechanisms imposing important forces.

Drag parameter quantification

The drag parameters (S_d and γ) were determined for each experimental seaweed using iterative, nonlinear least-squares curve fits of Eq. 2 to values of field-measured force (*via* Simplex methods, Press *et al.,* 1992; with fluid density, seaweed area, and velocity known). Use of this technique assumes that 100% of the measured force resulted from drag-related mechanisms, which is not strictly correct but is conservative and affected only weakly by brief transients tied to inertia and impingement. Potential "added mass" or "acceleration reaction" forces were neglected for the intertidal kelps on the basis of data from Gaylord (2000), and were ignored for the subtidal kelps because fluid accelerations are small in habitats outside the surf zone (Denny, 1988).

The least-squares method applied to Eq. 2 was used without modification to determine drag parameters for the *M. pyrifera* individuals tested subtidally. Determination of drag parameters for the intertidal *E. menziesii*, by contrast, incorporated processing adjustments to address two additional factors. First, because flows in the surf zone vary over spatial scales as small as or smaller than a few centimeters, wave-specific temporal offsets ($\approx$0.1 s) arose intermittently between the timing of wave arrival at the intertidal flow-and-force instruments. To minimize possible consequences for drag parameter estimation, the flow-and-force records were averaged over 0.5-s blocks, and the resulting smoothed traces of velocity and force were employed in the regressions used to determine S_d and γ. The second complication for the intertidal measurements was related to the fact that the *E. menziesii* individuals were often emergent. Because this situation led to the imposition of brief spikes in force at the instant of wave arrival (putatively due to impingement events), the first 0.5 s of the flow-and-force data from each wave were eliminated from the flow-force regressions. This protocol retained only the portions of wave passage characterized by full submergence of the experimental seaweeds and sensor apparatus (*i.e.,* those portions of the record where classic drag interactions would dominate, enabling accurate estimation of the drag parameters). With one exception discussed below, each of these two intertidal pro-

cessing adjustments was used only for estimation of the drag parameters, S_d and γ; otherwise the complete 50-Hz records of velocity and force were employed.

Quantification of predicted drag

The drag parameters calculated above were next reinserted with the measured velocity data and known projected areas back into Eq. 2, to predict the force distributions that would arise from drag. Due to reposturing effects, "going with the flow" behaviors, and slight temporal offsets between flow-and-force records caused by spatial separation of the field instruments, there was no expectation that drag distributions predicted on the basis of Eq. 2 would exactly match the measured force distributions. However, a key question was whether the observed deviations in measured force away from the drag predictions could be attributed primarily to kelp movement and/or spatial separation of the field instruments, or whether non-drag effects of impingement and inertia (which by Newton's Second Law had to operate at some level) also contributed appreciably to the total force. We approached this issue by focusing on the more extreme forces in the distributions, since such large deviations from the relationships of Eq. 2 were less obviously explained by instrumentation effects or seaweed reposturing.

Comparison of predicted drag and measured force across a range of seaweed size

Analysis of the extreme forces focused on relative magnitudes of specific force ratios across a range of seaweed size. Particular percentile values of total measured force were divided by corresponding percentile values of predicted drag, and these normalized forces (*i.e.,* force ratios) were examined to see if their magnitudes varied consistently as a function of seaweed size. If only drag-associated mechanisms of force imposition operated (including reposturing), there would be no underlying expectation for seaweed individuals of different size to exhibit different normalized forces. On the other hand, there are quite explicit predictions regarding size dependence of the normalized forces if one considers effects of wave impingement and organism inertia, and these patterns can be seen from the following two-phase analysis.

First, for each individual of both species, we aggregated all of the 10- or 20-min flow-and-force records tied to that individual. Second, for the aggregate intertidal data sets only, the initial 0.5 s of water velocity data for each wave was removed from consideration to avoid the known impingement artifacts in drag-sphere records that arise during wave arrival (Gaylord, 1999). An analogous 0.5 s of force data was removed from consideration at the end of each wave in the intertidal force data. This procedure maintained equivalent record lengths for velocity and force (an important criterion for subsequent calculations) while retaining the largest forces of greatest interest that occur during the impingement phase at the beginning of each wave.

Predicted drag was computed from the velocity data by using the drag parameters. Specific percentile values of measured force were then extracted and normalized by the corresponding percentile values of predicted drag, as follows. For each individual, a mean normalized force was calculated by dividing the mean field-measured force by the mean predicted drag. Higher percentile levels beyond the mean were also computed. The 95th percentile normalized force was quantified as the 95th percentile value of measured force, divided by the 95th percentile value of predicted drag. Analogous calculations were carried out for the 99th, 99.9th, and 99.99th percentile ranges. Values corresponding to the 99.99th percentile range reached to within approximately the 10th largest measurements in the sampled distributions.

Results

Drag parameters

The shape coefficients of drag (S_d) for *Egregia menziesii* decreased with the degree of "flatness" of the specimen, $A^{3/2}/V$ (Fig. 1A), as did S_d values for *Macrocystis pyrifera* (Fig. 1B). The latter canopy-forming species had much more frond area per seaweed mass, however, leading to much larger values of the flatness index. The drag exponent (γ) in *E. menziesii* declined with flatness index as well, although the significance of the correlation ($P < 0.05$) depended on one dominating point (the value of 0.466; Table 1). In *M. pyrifera*, γ was not significantly correlated with flatness index.

By determining S_d and γ from seaweeds deployed in a natural orientation in their native habitats, we obtained fits of Eq. 2 that accounted for an average of 38% of the total force variation on the *E. menziesii* individuals and 69% on the *M. pyrifera* individuals (example data in Fig. 2; summary statistics for all individuals in Table 1). The single individual for which there was a substantially lower level of correspondence (5% of the variance; Table 1) was the largest *E. menziesii* tested, which exhibited exceptional twisting, flapping, and whiplashing movements due to its great length (>3 m). Although some asymmetry of the residuals around the fits of Eq. 2 is also apparent in Figure 2, stepwise calculation of drag coefficients based on either the mean, median, or 84th percentile forces (median plus one standard deviation from a normal distribution) associated with a sequence of velocity bins spanning the range of measured flow speeds yielded the same general patterns as those that arose when using the least-squares estimates of S_d and γ.

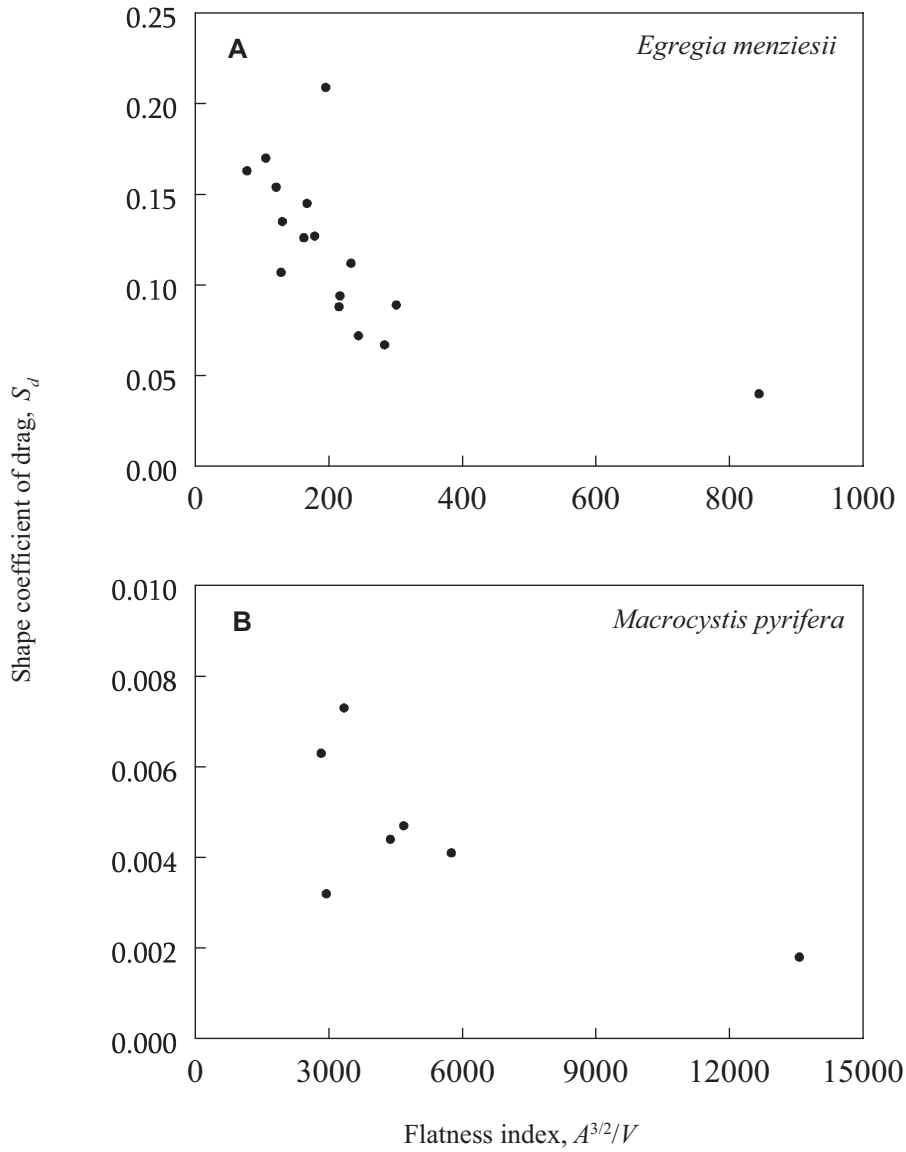

Figure 1. Shape coefficients of drag (S_d) for the (A) *Egregia menziesii* and (B) *Macrocystis pyrifera* individuals tested in the field, as a function of the "flatness index," $A^{3/2}/V$.

Patterns of intertidal and subtidal force

On a wave-by-wave basis, the flow forces acting on *E. menziesii* individuals exhibited a sawtooth pattern, where sharp impact-type spikes preceded more muted drag-based fluctuations in force (Fig. 3A). The temporal trajectories of the measured forces also mostly tracked the drag predictions that ensued from applying Eq. 2 to the measured velocities. The one temporal sector where the measured forces and the predicted drag diverged substantially in absolute magnitude was during the first instant of wave arrival (Fig. 3A). Many larger forces within this window were substantially in excess of those attributed to drag even if the drag-sphere velocity estimates within the initial 0.5 s after wave arrival were used to predict drag.

Force records for *M. pyrifera* in the subtidal zone (Fig. 3B) were quite different from those for *E. menziesii*. Although brief peaks in force were observed, the overall temporal pattern of force application did not exhibit a sawtooth trajectory. Rise-and-fall times of force were also not as brief as those seen intertidally. Force components explained by the predicted drag trajectory again represented a substantial portion, though not all, of the total force acting on the experimental *M. pyrifera* individuals.

Effects of length

The mean forces acting on the *E. menziesii* and *M. pyrifera* individuals increased strongly with the length of the individual (Fig. 4). This increase was essentially linear

Table 1

Drag parameters associated with Equation 2, determined for Egregia menziesii *and* Macrocystis pyrifera *individuals in the field; all the nonlinear regressions are significant at the $P < 0.001$ level*

Specimen	$S_d(m^{2-\gamma}\ s^{\gamma-2})$	γ	n*	r^2
E. menziesii				
1	0.170	1.404	1140	0.49
2	0.088	1.453	1140	0.43
3	0.072	1.301	954	0.35
4	0.107	1.004	962	0.32
5	0.163	1.220	1862	0.57
6	0.067	1.181	618	0.44
7	0.145	1.323	1595	0.48
8	0.112	1.239	1694	0.39
9	0.089	1.064	1486	0.19
10	0.135	1.088	1330	0.46
11	0.040	0.466	1387	0.05
12	0.127	1.134	1760	0.41
13	0.209	1.097	1643	0.33
14	0.094	1.098	988	0.30
15	0.126	1.198	1093	0.45
16	0.154	1.107	766	0.43
M. pyrifera				
1	0.0063	1.255	300	0.68
2	0.0047	1.246	300	0.78
3	0.0073	1.278	300	0.76
4	0.0018	1.083	300	0.73
5	0.0041	1.050	300	0.65
6	0.0044	1.152	300	0.76
7	0.0032	0.847	300	0.46

*The number of independent points, n, in each regression was calculated based on a 2-s decorrelation timescale for the intertidal measurements, and a 4-s decorrelation timescale for the subtidal measurements.

in *E. menziesii* but more scattered for *M. pyrifera*, owing to the latter species' tendency to proliferate its canopy when its fronds reach the water's surface. As a further consequence of increasing length, the fact that seaweeds cannot grow longer without adding area and mass means that both drag and inertial effects can be greater. In *E. menziesii*, which grows essentially as a strap, mass and maximal projected area increased with length at nearly the same rate, indicating that fronds retained a constant thickness as they got longer (Fig. 5). The modest elevation of the log-log slopes above 1.0 (*i.e.,* to values near 1.6) reflected the fact that longer individuals had a slight tendency to produce more and wider fronds. In the case of *M. pyrifera*, the slopes for how area and mass varied with thallus length were again not significantly different, although the rate at which these quantities increased with length was much higher than for *E. menziesii* (Fig. 5).

Large force transients acting on Egregia menziesii

When normalized forces were computed (*i.e.,* by dividing by the predicted drag and thus removing the attendant dependence on area), resultant patterns as a function of size in *E. menziesii* depended strongly on whether average or extreme forces were considered. The mean normalized force showed little if any trend with frond length (Fig. 6A). The trend changed dramatically, however, with peak forces (*i.e.,* forces in the 95th, 99th, 99.9th, and 99.99th percentile range). For such peaks, the curve of normalized force *versus* frond length acquired a U-shaped form, with greater normalized forces in shorter and longer *E. menziesii* than in individuals of intermediate length (Fig. 6B–E). For force extremes in the 99.99th percentile, actual peak forces in short and long individuals reached in excess of 3 times those predicted by the 99.99th percentile drag.

Large force transients acting on Macrocystis pyrifera

As with *E. menziesii*, mean normalized forces in *M. pyrifera* varied little with frond length (Fig. 7A), indicating that average forces tracked those expected from classic drag. For more extreme events (*i.e.,* forces in the 95th, 99th, 99.9th, and 99.99th percentile range), forces became increasingly large in longer individuals relative to predicted drag, exhibiting a J-shaped pattern (Fig. 7B–E). Normalized forces also increased more rapidly with length for forces at the higher percentiles. For example, force extremes in the 99.99th percentile range were as much as 3 times bigger than those associated with the 99.99th percentile drag. In contrast to the trends observed for *E. menziesii*, there was no tendency for smaller individuals to exhibit higher normalized forces.

Discussion

Uncertainties in the analyses

Portions of the intertidal drag-sphere records (4% to 6% of the data) were removed from consideration to avoid including known impingement biases in the velocity data. This procedure could have introduced inaccuracies, with two potential scenarios posing the greatest concern. First, there is the possibility that velocities always peaked during the first 0.5 s after wave arrival, and that important velocity values were therefore ignored during the analysis that led to Figure 6. However, although larger surf-zone velocities do tend to arise early (*i.e.,* within the first 1–2 s) during a wave's passage, Gaylord (1999) found that peak velocities retained after a processing procedure identical to the one used here either closely matched, or exhibited a lower bound consistent with, classic wave bore models. Had important velocity elements been eliminated, such a pattern would not have emerged. Second, it is possible that removing from consideration the 0.5-s force segments near the ends of waves biased the distribution of peak forces used to generate Figure 6. This second scenario also appears improbable. As can be seen in time-series records (Fig. 3A),

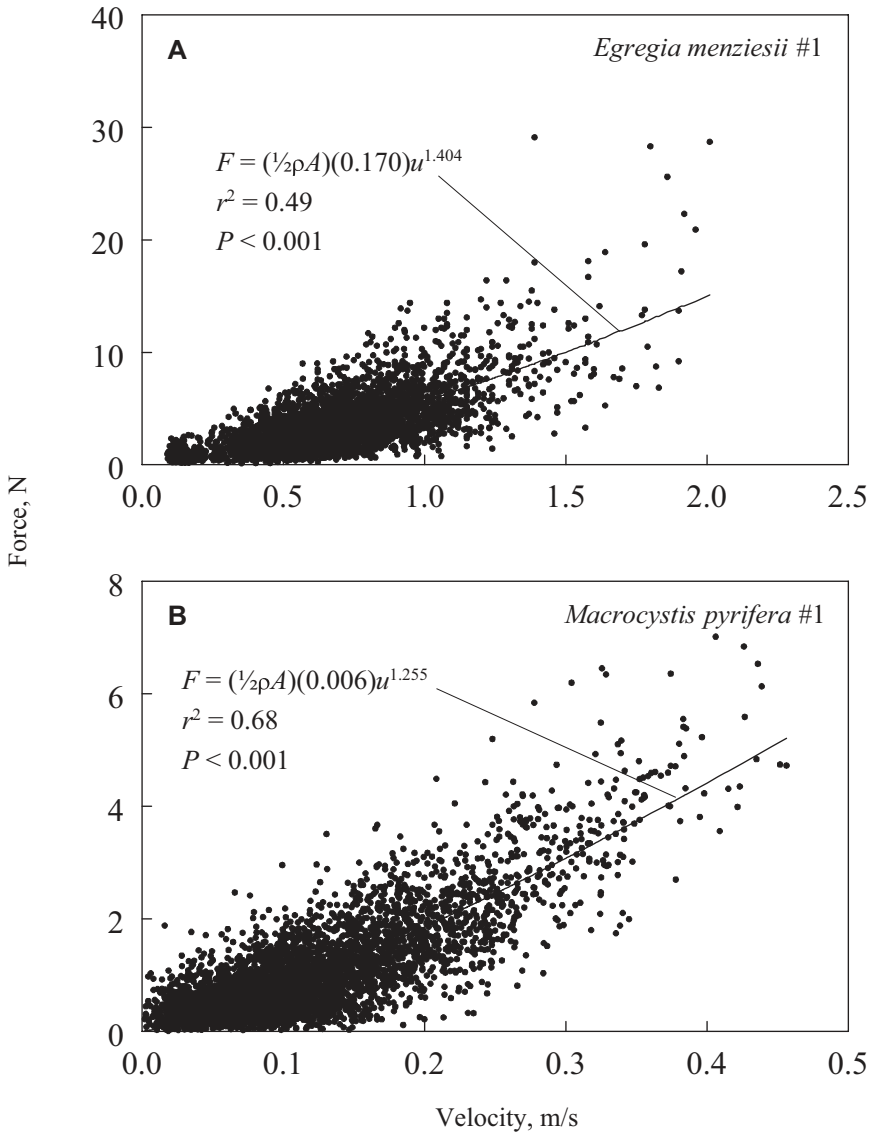

Figure 2. Example plots of measured force for (A) a representative *Egregia menziesii* specimen, and (B) a representative *Macrocystis pyrifera* specimen, *versus* measured velocity, demonstrating the fit of the drag expression of Eq. 2.

forces during the trailing portions of waves were small, and would therefore never have appeared in the higher-percentile curves of Figure 6. Although subtle changes in the exact percentile levels associated with specific force extremes could have arisen (shifting percentile values from 95th to 99th, or 99th to 99.9th, for example), Figure 6 would not be fundamentally different. Analogous procedures were not applied to the subtidal data and are thus irrelevant for evaluating Figure 7.

Drag parameters of large kelps as determined in the field

The present study is the first to measure drag parameters (S_d and γ) of seaweeds positioned in their natural orientations and habitats in the field, where flows are time-varying and disorganized. The results therefore validate the ability of standard drag expressions (originally developed for steady, unidirectional velocities) to model average forces applied to seaweeds in complex flows. Although the variance in force explained by Eq. 2 is modest (38%–69% for all specimens except one), tight regressions would be implausible under field conditions. Hence, the statistically significant fits of Eq. 2 to the field measurements bolster the long-held, but largely untested, assumption that elementary drag expressions can be used to infer routine fluid forces on flexible organisms in real habitats.

Data from the current study may also be valuable for

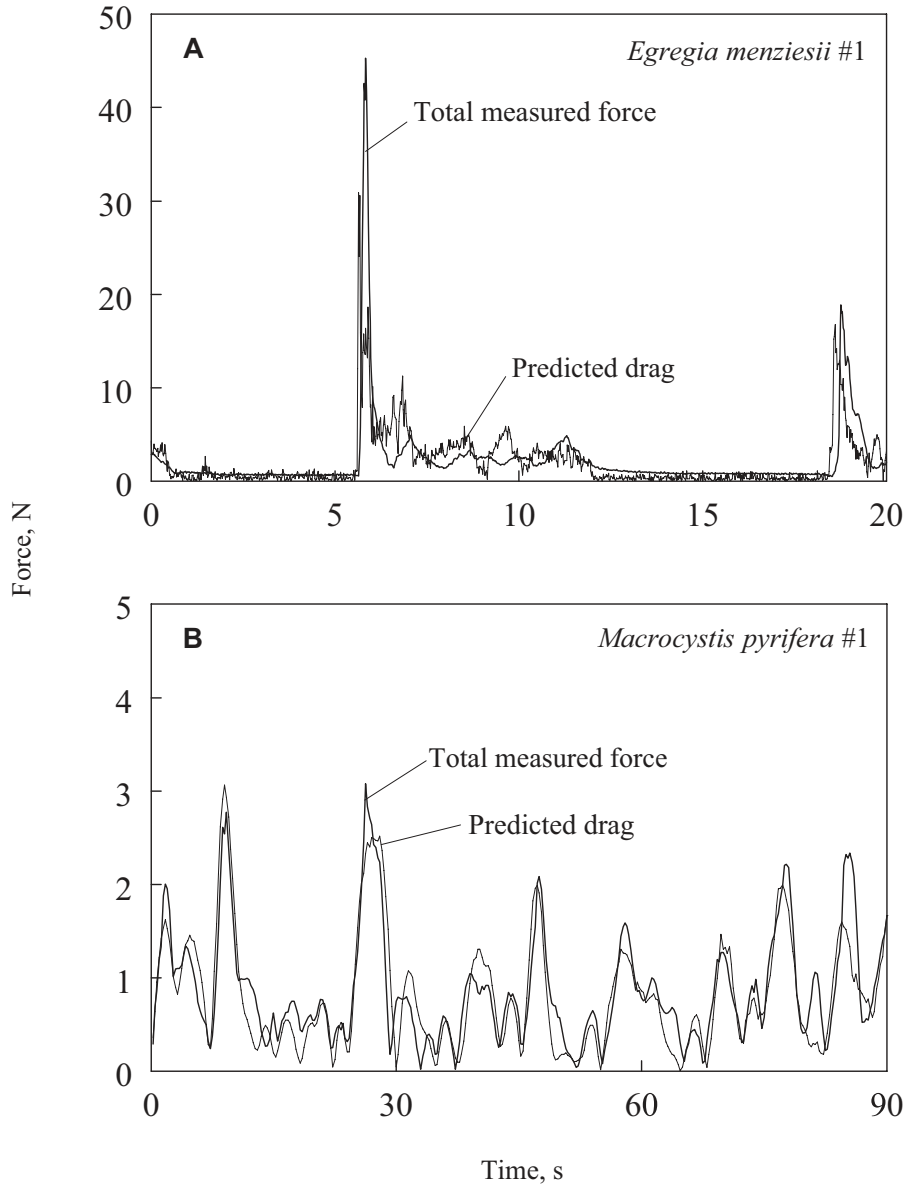

Figure 3. Time series of total measured force and predicted drag, for (A) a representative *Egregia menziesii* individual, and (B) a representative *Macrocystis pyrifera* individual. Note that predicted drag values during the first 0.5 s after wave arrival in (A) are dramatically overestimated due to impingement artifacts associated with drag-sphere probes (see text). The predicted drag values in such initial spikes are therefore discarded from other analyses of the study, and are presented here only to demonstrate that measured forces are still large relative to drag even if such overestimates are taken at face value. Deviations in measured force from predicted drag later in the wave are largely due to reposturing effects and the fact that drag is based on velocity measurements made 40 cm away from the location of the force measurements.

comparing field-measured values of S_d and γ to those determined using more traditional laboratory methods. Gaylord (2000) quantified coefficients and exponents of drag in accelerating flow for 12 species of intertidal seaweed, and found values of S_d that declined from about 0.2 at a flatness index of 1, to 0.07 at a flatness index of 200. The *Egregia menziesii* individuals of the present study exhibited nearly identical values for S_d across the same range of flatness index (Fig. 1A; Table 1). Values of γ for *E. menziesii* in the present study ranged from 1.00 to 1.45 across flatness indices from 1 to 200 (Table 1), somewhat lower than the γ values of 1.35 to 2.20 found by Gaylord (2000). The largest *E. menziesii* specimen tested in the present work exhibited much lower values of both S_d and γ than those reported by Gaylord (2000) but also had a far greater flatness index (Table 1). Only one other set of drag-parameter estimates is

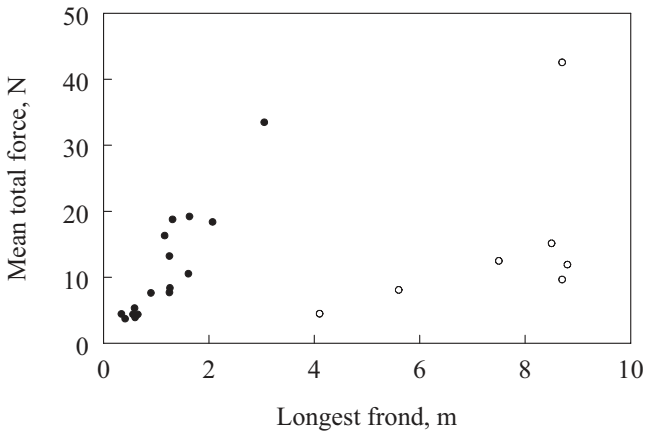

Figure 4. Relationship between the mean total force acting on a seaweed and the length of the seaweed's longest frond, for both *Egregia menziesii* (solid circles) and *Macrocystis pyrifera* (open circles).

available for *E. menziesii*, derived from measurements on a single individual of unknown flatness index tested in unidirectional, steady flow (S_d = 0.022, γ = 1.483; Friedland and Denny, 1995). Even fewer drag parameter values are available for comparison to the *Macrocystis pyrifera* data of the present study (Fig. 1B; Table 1). Utter and Denny (1996) towed from a boat an isolated *M. pyrifera* frond excised from the stipe bundle of a single individual, achieving values of S_d = 0.015 and γ = 1.596. Given that those authors employed only a small portion of the seaweed, it is unclear whether the roughly 2-fold difference between their estimate and the present set of S_d and γ values is significant.

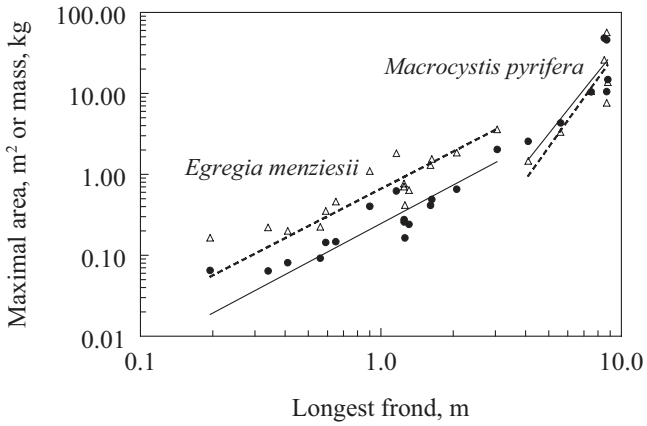

Figure 5. Allometric relationships between frond length and area or mass for *Egregia menziesii* and *Macrocystis pyrifera*, plotted on a log-log scale, derived using Reduced Major Axis methods (Sokal and Rohlf, 1995). Solid circles and solid lines indicate maximal projected area *versus* length data; open triangles and dashed lines indicate mass *versus* length data. *E. menziesii*: log(area) = 1.581 log(length) – 0.609, r^2 = 0.81; log(mass) = 1.529 log(length) – 0.178, r^2 = 0.79. *M. pyrifera*: log(area) = 3.729 log(length) – 2.105, r^2 = 0.70; log(mass) = 4.154 log(length) -2.568, r^2 = 0.74.

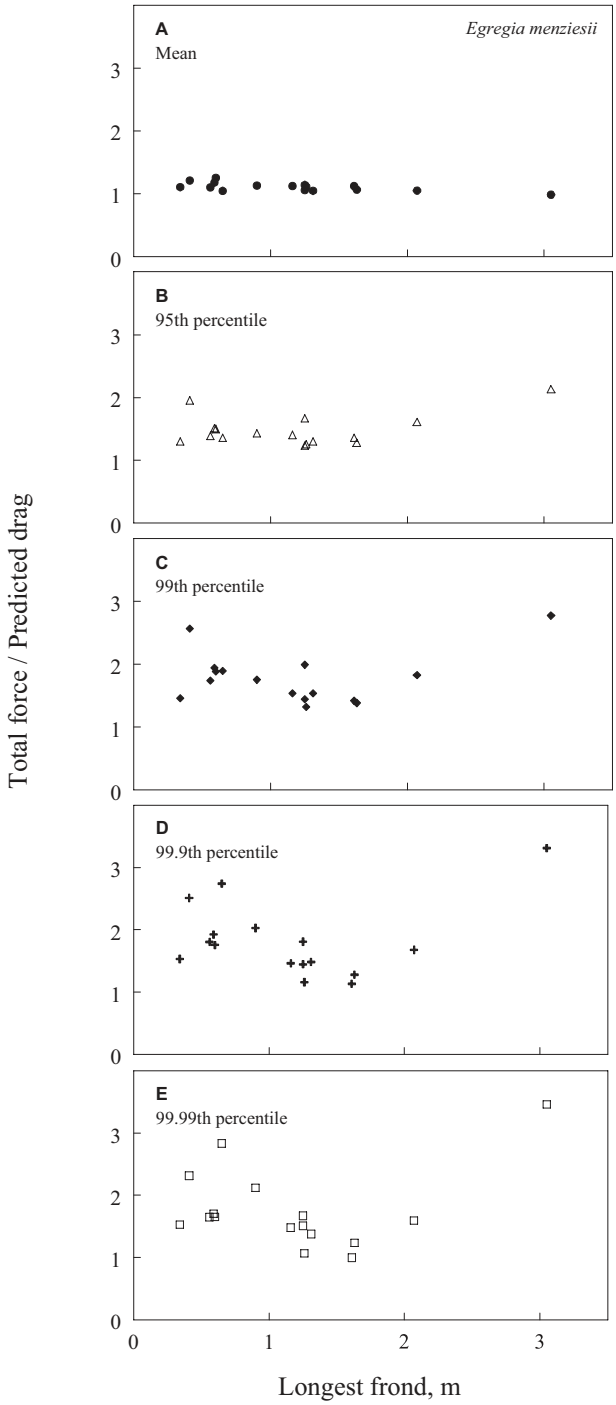

Figure 6. Normalized forces (specific percentile level of total measured force divided by the same percentile level of predicted drag) imposed on *Egregia menziesii*, as a function of the length of the longest frond. Note the U-shaped trajectory of the data points for the more extreme force percentiles, suggesting an increased vulnerability of both shorter and longer intertidal individuals to non-drag transients.

Consequences of flexibility as a function of organism size

The manner in which normalized forces (*i.e.,* total measured forces divided by predicted drag; Figs. 6 and 7) vary

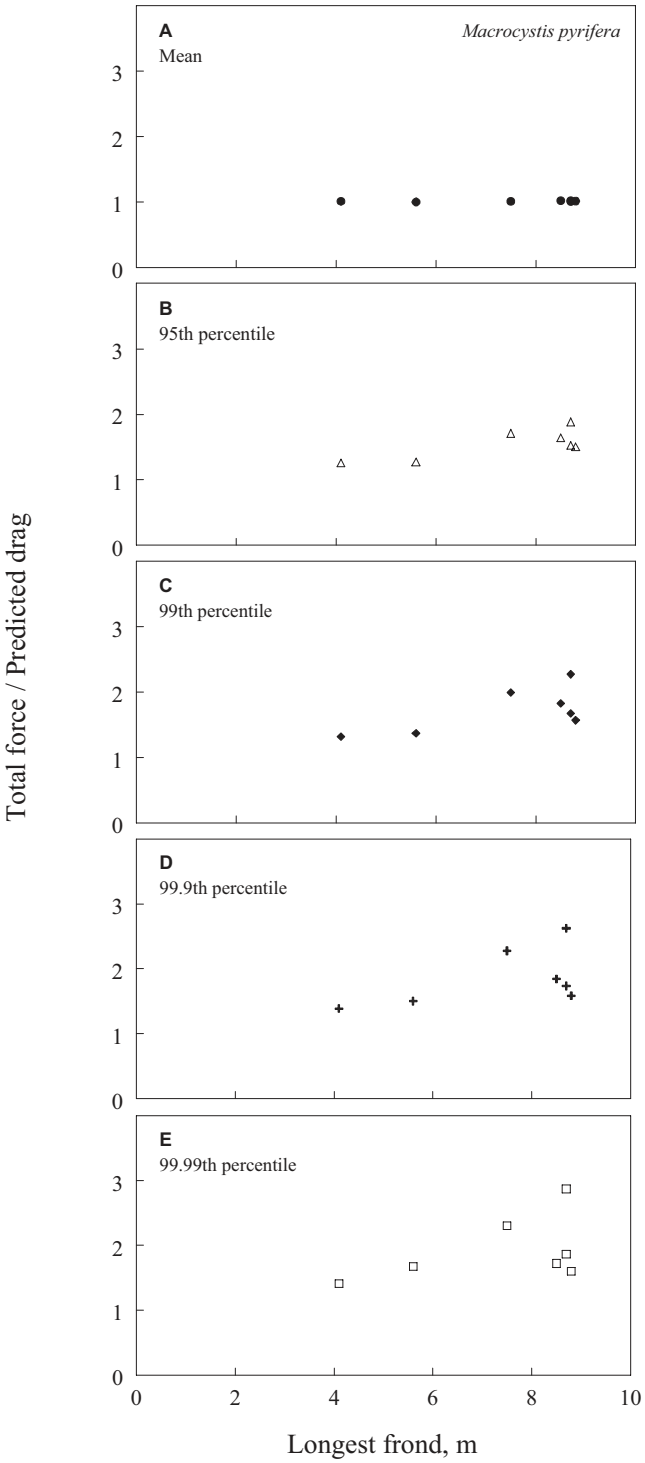

Figure 7. Normalized forces (specific percentile level of total measured force divided by the same percentile level of predicted drag) imposed on *Macrocystis pyrifera*, as a function of the length of the longest frond. Note the J-shaped trajectory of the data points for more extreme force percentiles, suggesting an increased vulnerability of longer subtidal individuals to non-drag transients.

as a function of plant length provides important clues to the origin of transient forces that act on flexible marine organisms of different sizes. A first observation is that length-dependent patterns in normalized force arise only for forces of larger magnitude. Mean forces track nearly exactly trends expected for drag, as evidenced by the clustering of normalized forces around 1.0 in Figures 6A and 7A. On the other hand, wave impingement and inertial effects, which act briefly and intermittently, would be expected to become increasingly apparent when exceptional values of force are considered. In the case of impingement events, they occur when the air-water interfaces of waves interact abruptly with appropriately oriented, emergent organisms (Gaylord, 2000). If a crisp air-water interface is absent, or if an organism is in a slack configuration at the instant of wave arrival (such that it must be reconfigured before being pulled taut), the impingement effect would be attenuated. Inertial effects would also be expected to emerge more robustly in analyses that resolve extreme, intermittent force transients. There would be no inertial "jerk" in a large individual that achieves substantial momentum but does not reach the end of its range of motion before slowing down (Gaylord *et al.,* 2003). The same seaweed, however, could experience a sizeable inertial force if wave-driven velocities at another instant became appropriately synchronized with the timing of canopy swaying.

The U-shaped pattern in force observed for *E. menziesii* is expected from effects of wave impingement and organism inertia. The tendency for smaller *E. menziesii* individuals to exhibit larger normalized forces (as represented by the left-hand arm of the U-curve) is consistent with smaller organisms having shorter mechanical response times, making them more vulnerable to brief fluid-dynamic transients. Larger individuals, by contrast, respond more slowly to brief transients (Gaylord *et al.,* 2001), enabling impingement events to expire before those events appreciably affect a seaweed. Inertial forces have an opposite relationship with size (Denny *et al.,* 1998; Gaylord, 2000). These forces depend on an organism's mass and so are negligible for small individuals, but they can be important for large ones. The right-hand arm of the *E. menziesii* U-curve is consistent with this latter trend. The remaining central dip in the curve can be interpreted as the size interval where neither impingement nor inertial forces dominate.

The J-shaped normalized force curve for *M. pyrifera* is also consistent with the above discussions of wave impingement and organism inertia. *M. pyrifera* resides in subtidal areas where breaking waves do not crash directly upon organisms, so wave impingement forces are not imposed. Inertial forces are active, however, and would be expected to become increasingly large in individuals of greater size.

The interpretations given in the preceding two paragraphs rely on the fact that patterns of peak force as a function of frond size (*i.e.,* Figs. 6 and 7) align with existing theories

regarding force imposition due to wave impingement and organism inertia. However, it is conceivable that other mechanisms could also generate similar U-shaped or J-shaped patterns of force as a function of seaweed size. For example, intermediate-sized *E. menziesii* individuals and small *M. pyrifera* individuals could experience reduced deviations in force from predicted drag as a consequence of some unanticipated organism-flow interaction. Such an explanation would demand that individuals change their response to flow in such a way that extreme forces decline only at intermediate size in one species, and only at smaller size in another, while simultaneously requiring that both species retain their monotonic increase in average force for large frond sizes. The existence of an undocumented mechanism of this type appears less likely than the impingement and inertia explanations already supported by theory. The similarities of the curves across each of the 95th, 99th, 99.9th, and 99.99th percentiles furthermore imply that the U- and J-shaped relationships are characteristic of substantial portions of the tails of the force distributions, and hence are not statistically ambiguous reflections of a few extreme points.

It is also possible that the patterns of Figures 6 and 7 could have arisen simply due to random variability among specimens in how each interacted with flow. This scenario can be assessed by comparison to a null model, where normalized force is independent of frond length. This situation can be represented by assuming an arbitrary collection of *E. menziesii* specimens characterized by 99.99th percentile normalized forces that follow a uniform distribution spanning values between 1 and 3.46 (the latter value set by the maximum measured normalized force). Samples corresponding in length and number to the specimens used in our study can be drawn from this distribution, and an assessment can be made of the probability that all of these samples would fall into a U-shaped parameter space similar to that occupied by our empirical data. For this analysis we used the parameter space shown in Figure 8A. Normalized force at mid-length was confined to the range 1–1.5. This central space was flanked by two boxes in which normalized force was confined to the range 1–2. Forces for very short or very long lengths were confined to the range 1.5–3.46. This parameter space loosely enclosed our data, and was U-shaped. Repeated random sampling of the null distribution revealed that there was less than a 0.001% chance that length-independent data would conform to the U-shape found in our empirical measurements. An analogous calculation for *M. pyrifera* (Fig. 8B), assuming in this case a uniform distribution of normalized force ranging from 1 to 2.87, yielded a probability of less than 3%. These probability values are also not sensitive to the precise shape of the assumed normalized force distribution. When rectified Gaussian distributions (Gaussians folded over to include only positive values) with standard deviations matched to the empirical *E. menziesii* or *M. pyrifera* data were assumed instead of a uniform distribution, a re-sampling analysis yielded probabilities that the U- or J-shaped curves would arise purely by chance of less than 0.02% and 2%, respectively. These probabilities are conservative in the sense that if the boxes of Fig. 8 were shrunk to encompass smaller U- or J-shaped regions that are also consistent with the data, the probability estimates would decline further.

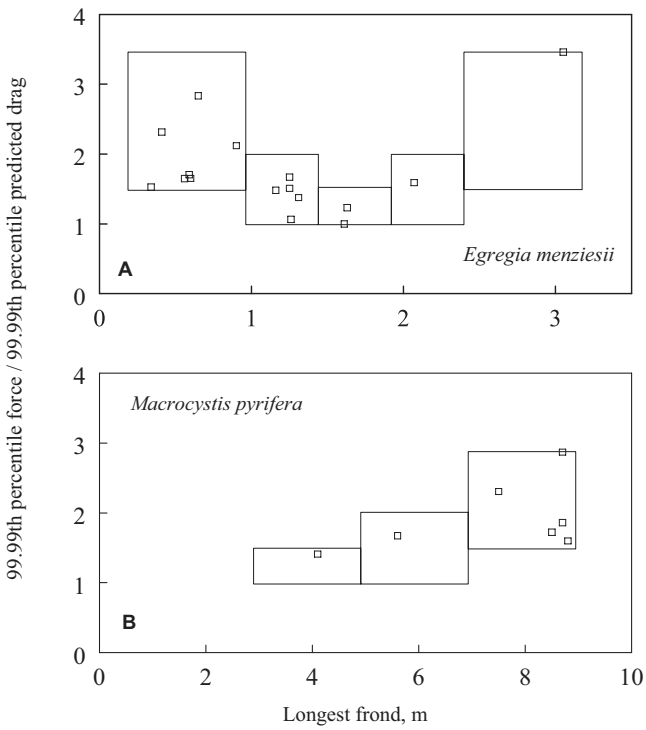

Figure 8. Conservative representation of the parameter space for normalized force that would reflect either (A) a U-shaped, or a (B) J-shaped relationship with seaweed size, for *Egregia menziesii* or *Macrocystis pyrifera*, respectively. The likelihood that the U- or J-shaped curves arose purely through chance can be quantified by computing the probabilities of all data points falling within the boxes shown, assuming that the force value for each seaweed length is drawn independently and randomly from the same (either uniform or Gaussian) distribution.

The observed U-shaped curve for the intertidal seaweeds can additionally be placed in the context of earlier computational work that examined the behavior of *E. menziesii* in flow. Employing idealized velocity fields that mimicked the dominant fluid structures found in surf-zone environments, Friedland and Denny (1995) predicted a near-linear increase in average force with stipe length. This pattern matches the trend found in our study (Fig. 4). Although the Friedland and Denny model did not examine stochastic flow events (*i.e.,* those associated with turbulence) that might contribute to the production of larger forces imposed on real organisms, and although their approach was unsuitable for evaluating wave impingement processes, it did predict that momentum-associated inertial forces would arise com-

monly in large individuals. This prediction is again consistent with what appears to be the simplest explanation for the right-hand portion of the U-curves observed with *E. menziesii* (Fig. 6).

Consequences of flexibility across intertidal habitats

The present study supplements prior work in revealing how wave impingement and inertial processes might interact with coastal topography. The field measurements of Koehl (1999) indicate that *Alaria marginata*, a ribbon-like intertidal kelp similar in some respects to *E. menziesii* (although it has only one sizeable frond) need not experience an increase in force with an increase in length, in contrast to the data of Figure 4. However, Koehl's measurements were conducted in surge channels subjected to less violent flows than those on the rocky outcrops of the present study. Her measurements also focused on seaweed individuals that remained exclusively underwater throughout each wave cycle. Immersed seaweeds in such channels are often not subjected to as sharp an initial onslaught of water, as evidenced by an absence of sawtoothed flow-and-force trajectories (Koehl, 1999). Under such circumstances, it is possible that mechanisms of "going with the flow" function more effectively to offset potential costs of increases in length associated with trends like those of Figure 4.

Effects of size and species interactions on dislodgement

There is a long tradition of interest in seaweed-flow interactions and their potential ability to limit distribution, morphology, and size in seaweeds. The present study provides empirical data on how flow forces vary across habitats and as a function of frond attributes. Force transients can get disproportionately large as seaweeds increase in size, even relative to drag-based forces that depend on frond area. As has been noted in prior studies (Carrington, 1990; Gaylord *et al.,* 1994; Kitzes and Denny, 2005), if such forces increase more rapidly with size than the ability of a species to withstand them, the risk of dislodgement may also increase with seaweed size. Further work examining the allometry of holdfast attachment strength could be valuable for evaluating this possibility.

Patterns of force imposition in *E. menziesii* and resultant implications for dislodgement may also be modulated by species interactions. In some locations, crowded groups of *E. menziesii* individuals exhibit higher rates of grazing by the limpet *Lottia insessa* (formerly *Acmaea insessa*), than do solitary individuals of *E. menziesii* (Black, 1974, 1976). *L. insessa* is a specialist consumer on *E. menziesii* that damages the seaweed's main axis and thereby causes distal tissue loss. Black (1976) proposed that limpet-induced pruning might reduce a seaweed's dislodgement probability by decreasing the frond area (and presumably the force imposed; Fig. 4) on an individual of given holdfast area. On the other hand, Black (1976) noted that solitary *E. menziesii* individuals supported fewer limpets and exhibited lower rates of pruning. While it is unclear whether grazing-induced shifts in projected area contributed to patterns of force observed in the present study, if consumer interactions generally influence dislodgement risk, they could have important demographic consequences for this species.

Dislodgement probabilities in *M. pyrifera* might be similarly coupled to its lifestyle. In subtidal areas where light levels are low at depth, there is considerable advantage for a buoyant kelp like *M. pyrifera* to grow to the water's surface. Subsequent proliferation of the canopy can then facilitate higher rates of photosynthesis, while simultaneously helping to shade out competitors. Increased canopy production also influences a number of interactions between the forest and flow (Gaylord *et al.,* 2004, 2006, 2007), some of which have costs. In particular, the production of a large canopy results in a greater projected area of frond, and thereby elevated forces. Under relatively severe hydrodynamic conditions, large *M. pyrifera* individuals may be at greater risk of dislodgement. High rates of winter mortality (Dayton and Tegner, 1984; Dayton *et al.,* 1992) and the almost complete loss of *M. pyrifera* in shallow water where waves break during storms (Seymour *et al.,* 1989; Graham, 1997) are a testament to the importance of physical disturbance in this organism's ecology.

Acknowledgments

We thank Brent Mardian, Clint Nelson, Shannon Harrer, and Bryce Wolcott for field assistance, and the Santa Barbara Coastal Long-Term Ecological Research program for logistical support. This work was funded by NSF grants OCE-0241447 and OCE-0523870 (to BG, MD, and MK); by the Virgina G. and Robert E. Gill Chair in Natural History (to MK); and by the Coastal Environmental Quality Initiative grant 04-T-CEQI-08-0048 administered by the University of California Marine Council (to BG). Contribution 2430 from the Bodega Marine Laboratory, University of California at Davis.

Literature Cited

Abbott, I. A., and G. J. Hollenberg. 1976. *Marine Algae of California*. Stanford University Press, Stanford.

Black, R. 1974. Some biological interactions affecting intertidal populations of the kelp *Egregia levigata*. *Mar. Biol*. **28:** 189–198.

Black, R. 1976. The effects of grazing by the limpet, *Acmaea insessa*, on the kelp, *Egregia laevigata*, in the intertidal zone. *Ecology* **57:** 265–277.

Blanchette, C. A., B. G. Miner, and S. D. Gaines. 2002. Geographic variability in form, size and survival of *Egregia menziesii* around Point Conception, California. *Mar. Ecol. Prog. Ser*. **239:** 69–82.

Boller, M. L., and E. Carrington. 2006. *In situ* measurements of hydrodynamic forces imposed on *Chondrus cripus* Stackhouse. *J. Exp. Mar. Biol. Ecol.* **337:** 159–170.

Carrington, E. 1990. Drag and dislodgment of an intertidal macroalga:

consequences of morphological variation in *Mastocarpus papillatus* Kutzing. *J. Exp. Mar. Biol. Ecol*. **139:** 185–200.

Dayton, P. K. 1972. Toward an understanding of community resilience and the potential effects of enrichments to the benthos at McMurdo Sound, Antarctica. Pp. 81–96 in *Proceeding of the Colloquium on Conservation Problems in Antarctica,* B. C. Parker, ed. Allen Press, New York.

Dayton, P. K., and M. J. Tegner. 1984. Catastrophic storms, El Niño, and patch stability in a Southern California kelp community. *Science* **224:** 283–285.

Dayton, P. K., M. J. Tegner, P. E. Parnell, and P. B. Edwards. 1992. Temporal and spatial patterns of disturbance and recovery in a kelp forest community. *Ecol. Monogr*. **62:** 421–445.

Denny, M. W. 1985. Wave forces on intertidal organisms: a case study. *Limnol. Oceanogr*. **30:** 1171–1187.

Denny, M. W. 1988. *Biology and the Mechanics of the Wave-swept Environment*. Princeton University Press, Princeton.

Denny, M. W. 1995. Predicting physical disturbance: Mechanistic approaches to the study of survivorship on wave-swept shores. *Ecol. Monogr*. **65:** 371–418.

Denny, M. W., and B. Gaylord. 2002. The mechanics of wave-swept algae. *J. Exp. Biol*. **205:** 1355–1362.

Denny, M. W., T. L. Daniel, and M. A. R. Koehl. 1985. Mechanical limits to size in wave-swept organisms. *Ecol. Monogr*. **55:** 69–102.

Denny, M. W., B. P. Gaylord, and E. A. Cowen. 1997. Flow and flexibility. II. The roles of size and shape in determining wave forces on the bull kelp *Nereocystis luetkeana. J. Exp. Biol*. **200:** 3165–3183.

Denny, M. W., B. Gaylord, B. Helmuth, and T. Daniel. 1998. The menace of momentum: dynamic forces on flexible organisms. *Limnol. Oceanogr*. **43:** 955–968.

Dudgeon, S. R., and A. S. Johnson. 1992. Thick vs. thin: thallus morphology and tissue mechanics influence differential drag and dislodgement of two co-dominant seaweeds. *J. Exp. Mar. Biol. Ecol*. **165:** 23–43.

Ebeling, A. W., D. R. Laur, and R. J. Rowley. 1985. Severe storm disturbances and reversal of community structure in a southern California kelp forest. *Mar. Biol*. **84:** 287–294.

Friedland, M. T., and M. W. Denny. 1995. Surviving hydrodynamic forces in a wave-swept environment: consequences of morphology in the feather boa kelp, *Egregia menziesii* (Turner). *J. Exp. Mar. Biol. Ecol*. **190:** 109–133.

Gaylord, B. 1999. Detailing agents of physical disturbance: wave-induced velocities and accelerations on a rocky shore. *J. Exp. Mar. Biol. Ecol*. **239:** 85–124.

Gaylord, B. 2000. Biological implications of surf-zone flow complexity. *Limnol. Oceanogr.* **45:** 174–188.

Gaylord, B., and M. W. Denny. 1997. Flow and flexibility. I. Effects of size, shape, and stiffness in determining wave forces on the stipitate kelps *Eisenia arborea* and *Pterygophora californica*. *J. Exp. Biol*. **200:** 3141–3164.

Gaylord, B., C. A. Blanchette, and M. W. Denny. 1994. Mechanical consequences of size in wave-swept algae. *Ecol. Monogr*. **64**: 287–313.

Gaylord, B., B. B. Hale, and M. W. Denny. 2001. Consequences of transient fluid forces for compliant benthic organisms. *J. Exp. Biol*. **204:** 1347–1360.

Gaylord, B., M. W. Denny, and M. A. R. Koehl. 2003. Modulation of wave forces on kelp canopies by alongshore currents. *Limnol. Oceanogr*. **48:** 860–871.

Gaylord, B., D. C. Reed, L. Washburn, and P. T. Raimondi. 2004. Physical-biological coupling in spore dispersal of kelp forest macroalgae. *J. Mar. Syst.* **49:** 19–39.

Gaylord, B., D. C. Reed, P. T. Raimondi, and L. Washburn. 2006. Macroalgal spore dispersal in coastal environments: mechanistic insights revealed by theory and experiment. *Ecol. Monogr*. **76:** 481–502.

Gaylord, B., J. H. Rosman, D. C. Reed, J. R. Koseff, J. Fram, S. MacIntyre, K. Arkema, C. McDonald, M. A. Brzezinski, J. L. Largier *et al.* 2007. Spatial patterns of flow and their modification within and around a giant kelp forest. *Limnol. Oceanogr*. **52:** 1838–1852.

Graham, M. H. 1997. Factors determining the upper limit of giant kelp, *Macrocystis pyrifera* Agardh, along the Monterey Peninsula, central California, USA. *J. Exp. Mar. Biol. Ecol*. **218:** 127–149.

Johnson, A. S., and M. A. R. Koehl. 1994. Maintenance of dynamic strain similarity and environmental stress factor in different flow habitats: thallus allometry and material properties of a giant kelp. *J. Exp. Biol.* **195:** 381–410.

Kitzes, J. A., and M. W. Denny. 2005. Red algae respond to waves: morphological and mechanical variation in *Mastocarpus papillatus* along a gradient of force. *Biol. Bull*. **208:** 114–119.

Koehl, M. A. R. 1977. Effects of sea anemones on the flow forces they encounter. *J. Exp. Biol*. **69:** 87–105.

Koehl, M. A. R. 1982. The interaction of moving water and sessile organisms. *Sci. Am.* **247:** 124–134.

Koehl, M. A. R. 1984. How do benthic organisms withstand moving water? *Am. Zool.* **24:** 57–70.

Koehl, M. A. R. 1986. Seaweeds in moving water: form and mechanical function. Pp. 603–634 in *On the Economy of Plant Form and Function,* T. J. Givnesh, ed. Cambridge University Press. Cambridge.

Koehl, M. A. R. 1999. Ecological biomechanics of benthic organisms: life history, mechanical design and temporal patterns of mechanical stress. *J. Exp. Biol*. **202:** 3469–3476.

Miller, L. P., and B. Gaylord. 2007. Barriers to flow: the effects of experimental cage structures on water velocities in high-energy subtidal and intertidal environments. *J. Exp. Mar. Biol. Ecol*. **344:** 215–228.

Press, W. H., S. A. Teukolsky, W. T. Vetterling, and B. P. Flannery. 1992. *Numerical Recipes in FORTRAN*. Cambridge University Press, Cambridge.

Seymour, R. J., M. J. Tegner, P. K. Dayton, and P. E. Parnell. 1989. Storm wave induced mortality of giant kelp, *Macrocystis pyrifera*, in Southern California. *Estuar. Coast. Shelf Sci.* **28:** 277–292.

Sokal, R., and J. Rohlf. 1995. *Biometry.* W. H. Freeman, New York.

Sousa, W. P. 1985. Disturbance and patch dynamics on rocky intertidal shores. Pp. 101–124 in *The Ecology of Natural Disturbance and Patch Dynamics,* S. T. A. Pickett and P. S. White, eds. Academic Press, New York.

Sousa, W. P. 2001. Natural disturbance and the dynamics of marine benthic communities. Pp. 85–130 in *Marine Community Ecology,* M. D. Bertness, S. D. Gaines, and M. E. Hay, eds. Sinauer Associates, Sunderland, MA.

Stevens, C. L., C. L. Hurd, and M. J. Smith. 2002. Field measurements of the dynamics of the bull kelp *Durvillaea antarctica* (Chamisso) Heriot. *J. Exp. Mar. Biol. Ecol*. **269:** 147–171.

Stewart, H. L. 2006. Ontogenetic changes in buoyancy, breaking strength, extensibility, and reproductive investment in a drifting macroalga *Turbinaria ornata* (Phaeophyta). *J. Phycol.* **42:** 43–50.

Utter, B. D., and M. W. Denny. 1996. Wave-induced forces on the giant kelp *Macrocystis pyrifera* (Agardh): field test of a computational model. *J. Exp. Biol*. **199:** 2645–2654.

Vogel, S. 1984. Drag and flexibility in sessile organisms. *Am. Zool*. **24:** 37–44.

Vogel, S. 1989. Drag and reconfiguration of broad leaves in high winds. *J. Exp. Bot*. **40:** 941–948.

Vogel, S. 1994. *Life in Moving Fluids*, 2nd ed. Princeton University Press, Princeton.

Wolcott, B. D. 2007. Mechanical size limitation and life-history strategy of an intertidal seaweed. *Mar. Ecol. Prog. Ser*. **338:** 1–10.